JOURNAL OF SPACECRAFT AND ROCKETS
Vol. 48, No. 3, May–June 2011

Linearized Aeroelastic Gust Response Analysis of a Launch Vehicle

Franco Mastroddi,* Fulvio Stella,† Davide Cantiani,‡ and Fabio Vetrano‡
University of Rome "La Sapienza," 00184 Rome, Italy

DOI: 10.2514/1.47268

A methodology for aeroelastic gust response of launch vehicles in flight is developed by using a previously validated aeroelastic stability analysis. The effects on the aeroelastic vibrations of a launch vehicle encountering a wind gust while operating at a particular supersonic flight condition are determined. A linearized dynamic aeroelastic analysis of the launch vehicles is performed using the previously developed procedure, but this time in supersonic flow. Then, the pressure on the moving launcher surface resulting from the combined motion induced by each elastic mode is obtained from the solution of the Euler equation. These effects are superimposed to determine the combined aerodynamic effects of all the modes. Thus, a generalized aerodynamic force matrix of the aerodynamic loads caused by the motion of the launch vehicles (rigid body, as well as elastic deformations) and the effect of a gust encountered in the flight is constructed. Finally, a generalized (iterative) eigenvalue analysis is performed to evaluate the aeroelastic stability of the linearized model of the launch vehicles, operating at the prescribed flow conditions, when it encounters a gust. This approach, along with the use the matched-filter theory on the resulting frequency response function, allows one to evaluate the effects of the worst-case excitation on the launch vehicle's aeroelastic response. The methodology has been applied to predict successfully the aeroelastic stability of LYRA launch vehicles when it flies through transverse gusts.

Nomenclature

A	=	amplitude parameter for Eq. (7), m
B	=	amplitude parameter for Eq. (18), m s^{-1}
C_p	=	pressure coefficient, dimensionless
$C_{p_n}^{\text{mot}}$	=	pressure coefficient field due to the motion of the n-th mode, dimensionless
C_p^{gust}	=	pressure coefficient field due to the gust, dimensionless
D, $[D_{mn}]$	=	damping matrix, kg m^2 s^{-1}
E, $[E_{mn}]$	=	generalized aerodynamic force matrix, m^3
e^{gust}, e_n^{gust}	=	aerodynamic unit gust vector, m^2 s
$e_n(t)$	=	n-th generalized aerodynamic force, kg m^2 s^{-2}
f_n^{gust}	=	n-th generalized gust force, kg m^2 s^{-2}
$H(\omega)$	=	generic frequency response function
$h(t)$	=	generic impulsive response function
K, $[K_{mn}]$	=	stiffness matrix, kg m^2 s^{-2}
$\mathbf{k}$	=	unit vector orthogonal to the launch vehicle axis, dimensionless
M, $[M_{mn}]$	=	mass matrix, kg m^2
M_∞	=	undisturbed flow Mach number, dimensionless
$\mathbf{n}$	=	unit normal vector outward the launch vehicle body surface, dimensionless
$q_n(t)$	=	Lagrangian coordinates, dimensionless
q_D	=	dynamic pressure, Pa
$q_m^t(t)$	=	input trial function associated to the m-th mode, m
S	=	body surface, m^2
s	=	Laplace domain variable, rad s^{-1}
T	=	time-window width, s
U_∞	=	undisturbed flow speed, m s^{-1}
$\mathbf{u}$	=	displacement field, m
$\mathbf{u}^{(n)}$	=	displacement field induced by the n-th mode shape, m
$\mathbf{v}$	=	fluid velocity vector field, m s^{-1}
$\mathbf{v}^{\text{gust}}$	=	gust velocity vector field, m s^{-1}
$\mathbf{v}^{\text{mot}}$	=	fluid velocity vector field induced by launch vehicle motion, m s^{-1}
$w(t)$	=	transverse component of the gust profile, m s^{-1}
$w^t(t)$	=	input trial functions for the identification of the unit gust vector, m s^{-1}
$\mathbf{x}(\xi^\alpha, t)$	=	position vector field, m
$x^m(t)$	=	generic input for the matched-filter theory, dimensionless
$y^m_{m_{\max}}$	=	generic worst response, dimensionless
α	=	launch vehicle angle of attack, deg
δ_{mn}	=	Kronecker delta symbol
$\varepsilon_h(t)$	=	energy associated to the generic impulse response $h(t)$, dimensionless
ε_x	=	energy associated to the generic input function $x(t)$, dimensionless
ζ_n	=	n-th damping-ratio coefficient, nondimensional
κ	=	smoothness control coefficient, dimensionless
ξ^α	=	α-th material coordinates, m
ρ_∞	=	undisturbed air mass density, Kg m^{-3}
$\mathbf{\Psi}^{(n)}$	=	n-th modal shape function, m
ω	=	Fourier-domain variable, rad s^{-1}

Received 19 September 2009; revision received 18 November 2010; accepted for publication 17 January 2011.

*Associate Professor, Department of Aerospace Engineering and Astronautics, Via Eudossiana, 18.

†Associate Professor, Department of Mechanics and Aeronautics, Via Eudossiana, 18.

‡Aerospace Engineering, Department of Aerospace Engineering and Astronautics, Via Eudossiana, 18.

I. Introduction

FIXED-WING aeroelasticity has been thoroughly studied for the whole of the history of aviation. Hence, that there is a rich vein of research developed over more than 100 years, [1], whereas launch vehicle (LV) aeroelasticity have only been of interest for the last 50 years. The main methodological developments of aeroelastic analysis of fixed wings were reached by means of improvements in its basic models, namely, by improvements of unsteady potential flow modeling [2] and the development of the linear analysis of vibrations of structures. Since the main theoretical constructs underpinning the two techniques are widely accepted and satisfied in most of flight conditions of both civil and military aircraft, the above

approach has became an unquestioned state of the art. This is illustrated by the large number of methods that have been developed for linear aeroelastic stability and response analysis [1,3–7] and by the fact that these procedures are actually available in several commercial codes [8]. Unfortunately, in a number of cases there are conditions that preclude the acceptance of these hypotheses. These include stall, transonic flows, flows in which viscous effects are important, and large deformations of structures. For such cases two methods of obtaining a solution have been generally successfully used for both fixed wings and rotary wings aircraft.

The first approach consists of the coupled solution of the Navier–Stokes equations (obtained with a computational fluid dynamics, or CFD, solver) and of the equations for the dynamics of the structure (by a finite element, or FE, solver). As might be expected, one needs suitable boundary conditions at the interface that effectively represent the appropriate fluid/structure interactions. This approach, although probably the closest to physical reality, is difficult to use since, due to the nonlinearity of the problem, the stability boundary might depend upon the initial conditions. As consequence, a large number of simulations have to be performed, at least in principle, to explore all the possible initial conditions of the aeroelastic system corresponding to stability. It follows that this approach is expensive in terms of the CPU time required to obtain a solution, thus making it not appealing in practical applications. The lack of experimental tests on the aeroelasticity of launch vehicles [9–16] was the motivation, for example, for Karpel et al. [13] adopting direct numerical simulations. As pointed out above, this approach is quite demanding in terms of human and computational resources and is therefore not practically usable in the designing phase of LVs.

The second approach employs a linearization of the flow-structure interaction around a prescribed reference flight condition to significantly simplify the problem thereby greatly reducing the computational burden. This linearization might be performed either by a mathematical linearization of the original partial differential equations of the model (e.g., a transonic small disturbance model for the aerodynamics) with the successive discretization in space and time; or by means of a numerical linearization of the aerodynamic numerical model by using a CFD code as a black box producing data for the needed numerical derivation [4,17,18]. Specifically, following this linearization approach, the aeroelastic analysis of a 3-D geometry of a LV in the neighborhood of a given transonic flight condition with prescribed angles of attack was successfully conducted by Capri et al. [17] and by Mastroddi et al. [18]. Further, Capri et al. [17] developed a structural dynamic model using a linear modal representation for the LV structure in terms of the lower natural frequencies and natural modes of vibrations. The linearized unsteady aerodynamic model was obtained by using CFD data given by an Euler code that was postprocessed to obtain a global generalized representation of the unsteady aerodynamic loads based upon imposed modal deformations of the LV. A linearized aerodynamic operator was then identified through a time/frequency domain system-identification approach based on giving a trial unsteady-boundary-condition input expressed in terms of shapes given by the modal analysis of the LV structure. Both the structural and the linearized aerodynamic models were finally employed in the linearized aeroelastic coupled model given by the generalized Lagrange equations of motion to verify the local aeroelastic stability of the European single-body multistages launcher VEGA.

This approach was extended by Mastroddi et al. [18] by performing a sensitivity analysis of the resulting aeroelastic stability margins as a function of mesh discretization, number and type of mode shapes, angle of attack, Mach number, flight speed, and air density. This analysis confirmed the predictive capability of the approach as an effective and accurate tool for the aeroelastic analysis of LVs. The procedure was essentially based on a CFD recalculation and updating of the aerodynamic database for several flight conditions. Further, in a previous work, Mastroddi et al. [19] adopted an unsteady aerodynamic for aeroelastic sensitivity analysis. The computational efficiency of this approach is good.

In the present paper, the linearizing procedure for the aeroelastic system identification of a LV developed by Capri et al. [17] and also applied by Mastroddi et al. [18,19], has been extended and applied to gust response problems of LVs. Unlike aircraft, there is no regulation defining an acceptable gust scenario for LVs. Therefore, testing the response performance with a worst-case scenario (for a given rms energy) appears the only acceptable procedure. This may be achieved by using the matched-filter theory (MFT) [20–22]. Specifically, such a theory may be employed to predict the highest acceleration of the aeroelastic response for a particular energy level of the input (represented, for example, by the root mean square of the energy of the input time signal). In the present study the linearized gust frequency response function is identified and then applied, by the use of the MFT, to predict the highest response of the LYRA LV configuration.

Although the development of the linearization procedure has been previously presented for a LV in transonic flight [17], it is summarized in Sec. II as it forms the theoretical basis of the linearization procedure in Sec. III, which extends the formulation to the prediction of the effects of a gust encountered by a LV in supersonic flight. This is followed in Sec. IV by some theoretical remarks on the application of the MFT to gust response problem. In Sec. V the numerical results on aeroelastic stability and response, including the worst-case scenario of LYRA LV are presented. Finally, in Sec. VI some conclusions are pointed out.

II. Theoretical Model for Linearized Aeroelasticity

Let us introduce the basic equation for the linearized aeroelastic stability of a LV. The linearized motion with respect to an equilibrium position of an elastic body in a external flow is described in the Laplace domain by the generalized Lagrange equations of motion [1]

$$\sum_{m}^{N} s^2 M_{nm}\tilde{q}_m + \sum_{m}^{N} sD_{nm}\tilde{q}_m + \sum_{m}^{N} K_{nm}\tilde{q}_m = q_D \sum_{m}^{N} E_{nm}(s; M_\infty, U_\infty, \alpha)\tilde{q}_m + \tilde{f}_n^{\text{gust}} \tag{1}$$

where the tilde symbol˜denotes the Laplace transform with respect to time; q_n are the generalized Lagrangian modal coordinates, K_{nm} is the modal stiffness matrix, M_{nm} is mass matrix, D_{nm} is the modal damping matrix with $D_{nm} := 2\zeta_m\sqrt{K_{mm}M_{mm}}\delta_{nm}$ and where δ_{nm} is the Kroneker symbol, $q_D := \frac{1}{2}\rho_\infty U_\infty^2$ is the dynamic pressure, ρ_∞, U_∞, M_∞ are the fluid density, velocity, and Mach number of the undisturbed flow, respectively, E_{nm} are the elements of the linearized unsteady aerodynamic matrix operator (generalized aerodynamic force matrix, or GAF, typically dependent on the Laplace variable s and the flow conditions M_∞, U_∞ and the LV steady angle of attack), $\tilde{f}_n^{\text{gust}}$ is the generalized aerodynamic modal gust load vector. The diagonal modal matrices M, K, and D are typically determined by a FE analysis and N is the number of modes assumed in the analysis so as to describe the aeroelastic displacement field of the body by

$$\mathbf{u}(\xi^\alpha, t) = \sum_{m}^{N} q_m(t)\boldsymbol{\Psi}^{(m)}(\xi^\alpha) \tag{2}$$

where $q_m(t)$ are the Lagrangian modal coordinates, ξ^α ($\alpha = 1, 2, 3$) are material coordinates, and $\boldsymbol{\Psi}^{(m)}(\xi^\alpha)$ the set of the assumed modes.

The GAF matrix E in Eq. (1) can be identified by an input/output procedure [17]. When the motion of the body surface is prescribed, it may be represented in terms of the Lagrangian coordinates $q_m(t)$. The consequent impermeability condition may be applied to the fluid boundary of the solid/fluid interface. Specifically, in view of the fact that the analysis is linear, we can address one mode at the time. Thus, if the motion is determined only for the generic m-th mode $\boldsymbol{\Psi}^{(m)}$, the corresponding body (LV) displacement field will be given by [see Eq. (2)]

$$\mathbf{u}^{(m)}(\xi^\alpha, t) = q_m^t(t)\boldsymbol{\Psi}^{(m)}(\xi^\alpha) \tag{3}$$

where $q_m^t(t)$ is an arbitrary function of time that represents the time dependence of the motion given in the space domain by the m-th

Table 1 Natural frequencies of the first four pairs of modes employed in the analysis (*B* = Bending, PL = PayLoad)

Mode types	Dimensionless natural frequencies
I B	1.00
II B	3.58
III B-PL	4.93
PL	5.17

modal shape. Therefore, the updated position $\mathbf{x}(\xi^\alpha, t)$ of the generic LV material point, with material coordinate ξ^α after the time dt, is given by

$$\mathbf{x}(\xi^\alpha, t + dt) = \mathbf{x}(\xi^\alpha, t) + \mathbf{\Psi}^{(m)}(\xi^\alpha)\dot{q}^t_m(t)dt \tag{4}$$

Then, assuming that Eq. (4) describes the motion of the mesh on the surfece of the vehicle, the corresponding pressure coefficient field $C^{\text{mot}}_{p_m}(\xi^\alpha, t)$ can be numerically evaluated by means of the CFD code once the boundary conditions associated with Eq. (3) are assigned and the reference steady pressure field resulting from the steady supersonic motion of launcher is filtered out from the aerodynamic load. Consequently, the n-th generalized aerodynamic force is given by the projection on the external LV surface S of the n-th mode on the evaluated pressure field, or

$$e^m_n(t) = -q_D \oiint_S C^{\text{mot}}_{p_m}(\xi^\alpha, t)\mathbf{n} \cdot \mathbf{\Psi}^{(n)}(\xi^\alpha)\, \mathrm{d}S \tag{5}$$

in which $\mathbf{n}$ is the outward unit normal to the body surface. After transforming this force in the Laplace domain, the GAF matrix can be written as

$$E_{nm}(s; M_\infty, U_\infty, \alpha) = \frac{\tilde{e}^m_n}{\tilde{q}^t_m q_D} \tag{6}$$

The choice of the function $\tilde{q}^t_m$ is in principle arbitrary, but this choice has an important effect on time/frequency transformation issues and CFD time/space discretization. Indeed, the $\tilde{q}^t_m$ function has to be a sufficiently narrow pulse in time with a consequent large frequency spectrum to excite all the modes included in the aeroelastic analysis. At the same time, it cannot have too large a frequency band. This fact may lead to numerical instabilities in the CFD solver. Thus, the Gaussian function

$$q^t_m(t) = A_m e^{-[(t-\frac{T}{2})/\kappa T]^2} \tag{7}$$

is ideal for this purpose. Here, A_m is the impulsive function amplitude, T is the time window width, and κ (with $0 < \kappa < 1$) is a coefficient controlling the smoothness of the function at the boundary of its time domain [17]. Then, using the Eq. (6), the GAF matrix, that is, the linearized unsteady aerodynamic operator $\mathsf{E}(s; M_\infty, U_\infty)$, is identified.

Note that a stability analysis on the linearized system may be performed by evaluating the values s_n such that

$$\det[s^2_n \mathsf{M} + \mathsf{K} - q_D \mathsf{E}(s_n; M_\infty, U_\infty, \alpha)] = 0 \tag{8}$$

where the parametric dependences of the GAF matrix E, are clearly demonstrated [17,18]. Having established the aerodynamic generalized forces, it is now possible to evaluate the effect of a gust on the aeroelastic vibration of a LV.

III. Modeling of the Aeroelastic Response to a Gust Input

The presence of an atmospheric disturbance given by a transverse gust in flight can be modeled by considering the relative motion of the LV with respect to the transverse perturbing gust. A number of assumptions need to be made to make the problem tractable. First, as is usual in aeroelasticity, the LV length is assumed to be small in comparison with the characteristic length of the gust profile. This means that the gust profile, prescribed in terms of gust velocity $\mathbf{v}^{\text{gust}}$,

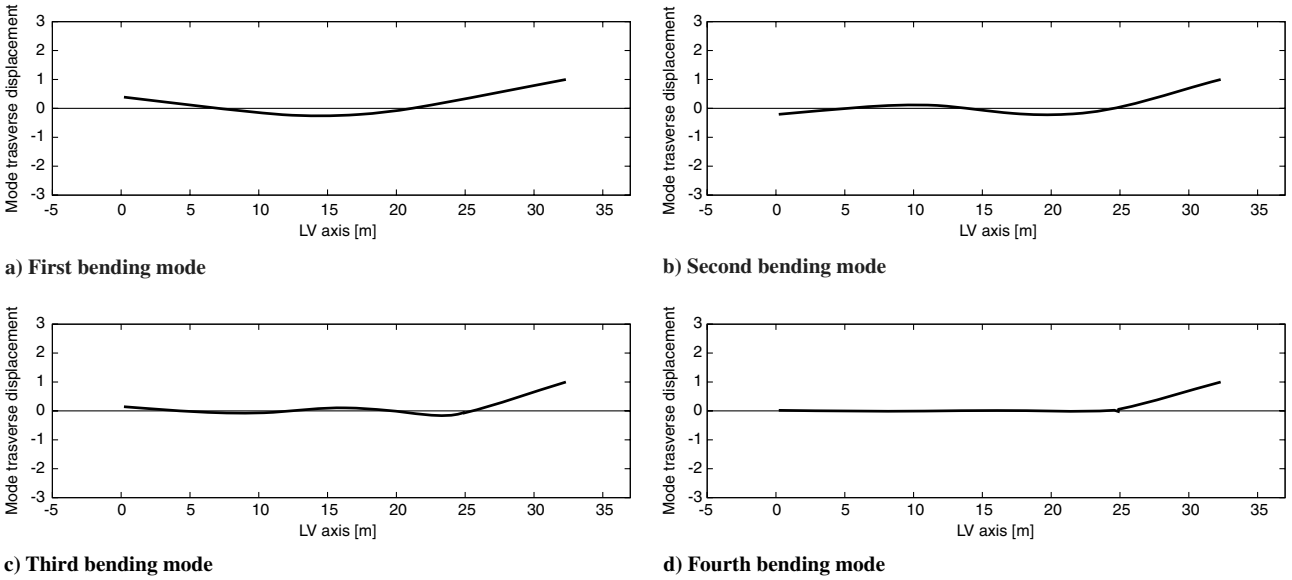

Fig. 1 Four free–free bending modes of the sticklike LV model: normalized transverse displacement as function of axial position (maximum displacement is on the nose of LV).

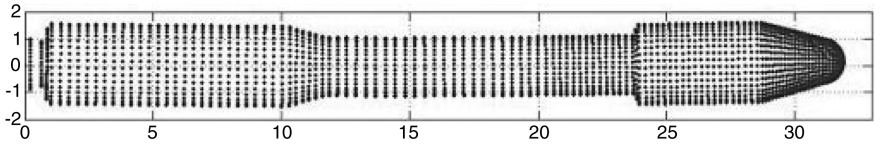

Fig. 2 Surface-expanded first mode shape of the LV 3-D model.

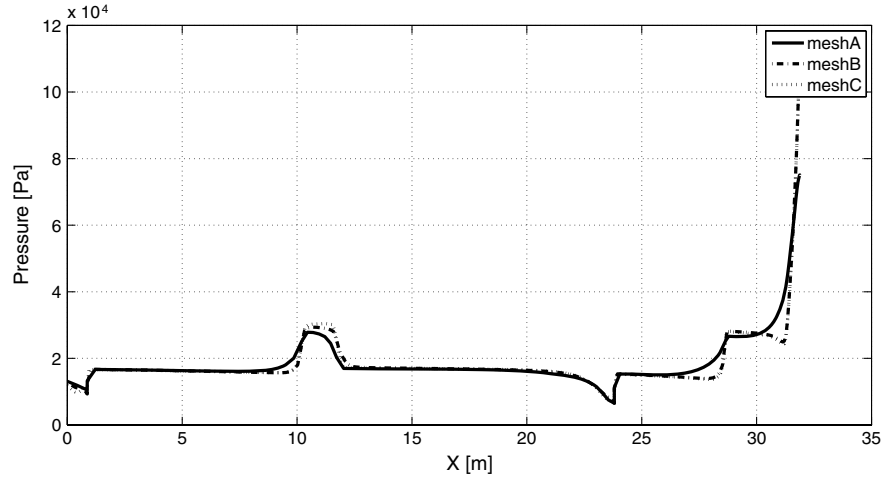

Fig. 3 Mesh sensitivity. Steady pressure distribution on the launcher surface: mesh $A = 3 \times 10^5$ cells, mesh $B = 6 \times 10^5$ cells, and mesh C 12 $\times 10^5$ cells.

is frozen, i.e., in the undisturbed air frame of reference with space coordinates $\mathbf{x}_A = (x_A, y_A, z_A)$:

$$\mathbf{v}^{\text{gust}}(\mathbf{x}_A, t) = \mathbf{v}^{\text{gust}}(\mathbf{x}_A) \tag{9}$$

so that the LV aerodynamics does not influence the velocity distribution within the gust. Further, the velocity $\mathbf{v}^{\text{gust}}$ does not depend upon the transverse direction. Further, because the launcher is small relative to the gust, the gust model is based on the assumption that the gust disturbance is uniformly distributed over all the LV surface as the vehicle passes through the gust, or, in the body frame of reference $\mathbf{x}_B = (x_B, y_B, z_B)$

$$\mathbf{v}^{\text{gust}}(x_B) = \mathbf{v}^{\text{gust}}(x_B - U_\infty t) = \mathbf{v}^{\text{gust}}(t) \tag{10}$$

Indeed, as it is typical to be assumed for the aeroelastic gust response theory of aircraft, the characteristic length of the turbulence able to

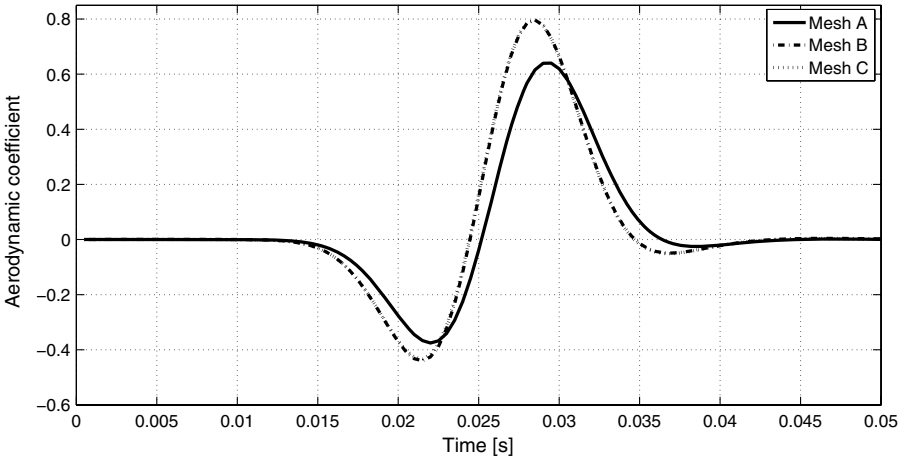

a) Generalized force 1 as due to the motion of the mode 1

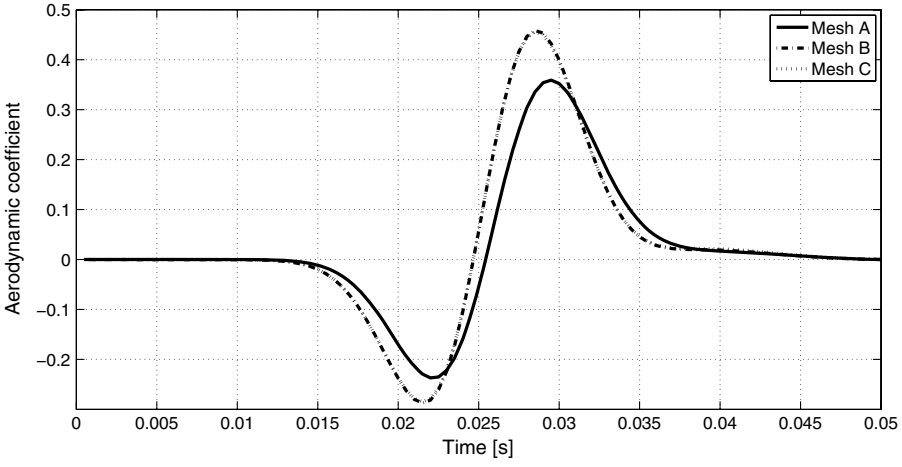

b) Generalized force 2 as due to the motion of the mode 1

Fig. 4 Mesh sensitivity. Study on the generalized force 1 and 2 as due to the motion of the mode 1.

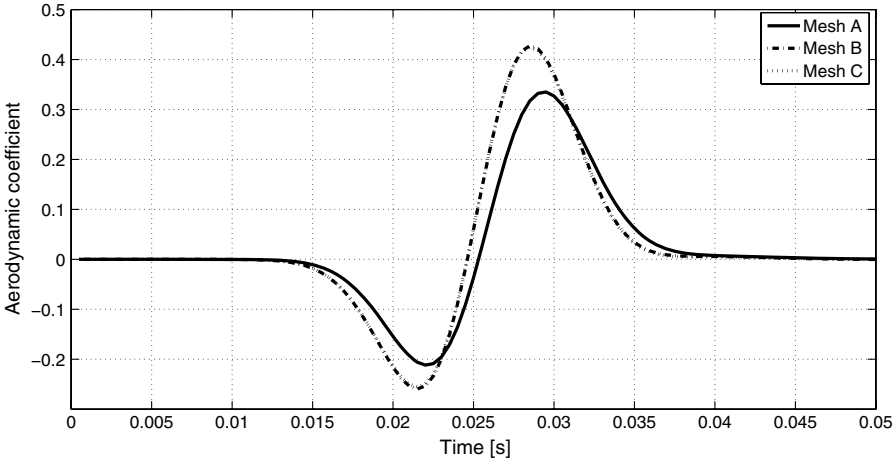

a) Generalized force 3 as due to the motion of the mode 1

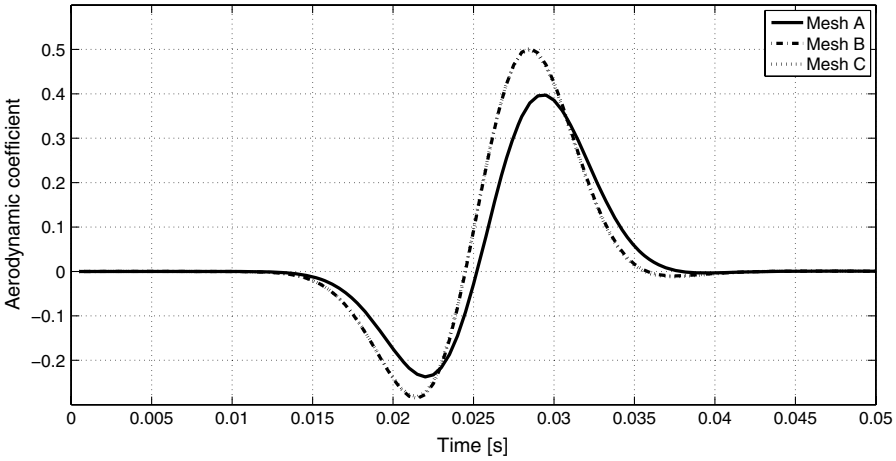

b) Generalized force 4 as due to the motion of the mode 1

Fig. 5 Mesh sensitivity. Study on the generalized force 3 and 4 as due to the motion of the mode 1.

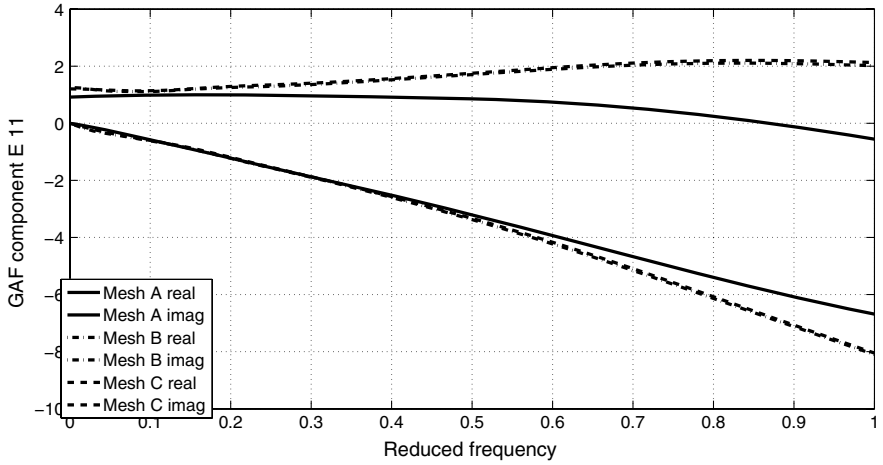

Fig. 6 Mesh sensitivity on the component E_{11} of the GAF in frequency domain (as function of the reduced frequency k).

influence transversally the motion and the deformation of the aircraft, is greater the characteristic longitudinal length of the aircraft. This aspect induce to assume the gust to be longitudinally uniform along the LV axis at any time.

Finally, the gust is supposed to be purely transverse to the LV, i.e.

$$\mathbf{v}^{\text{gust}}(t) = \mathbf{k}\, w(t) \tag{11}$$

Table 2 Dimensionless aeroelastic poles in the reference studied flow conditions

Poles	Real part	Imaginary part	Damping coefficient
#1	−1.00	63.03	1.74
#2	−3.29	227.65	1.25
#3	−3.94	315.49	1.44
#4	−5.69	326.57	1.62

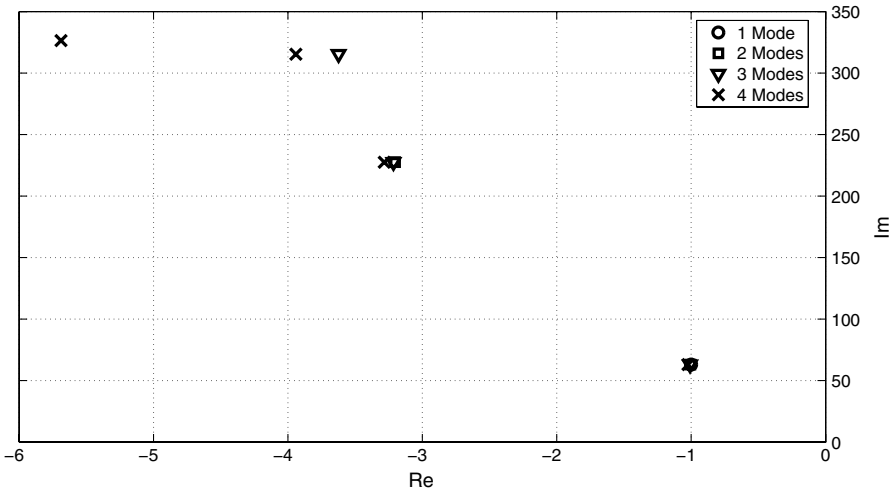

Fig. 7 Aeroelastic poles of LV considering 1, 2, 3, and 4 modes in the linearized aeroelastic stability analysis.

where $w(t)$ is the prescribed transverse component of the gust profile and $\mathbf{k}$ is a unit vector orthogonal to the LV axis.

Thus, the influence of the gust profile on the flow boundary conditions on the surface of the LV is given by

$$\mathbf{v}_B \cdot \mathbf{n} = \mathbf{v} \cdot \mathbf{n} \tag{12}$$

where $\mathbf{v}_B$ is LV velocity of the body structure so that

$$\mathbf{v} = \mathbf{v}^{\text{gust}} + \mathbf{v}^{\text{mot}} \tag{13}$$

in which $\mathbf{v}$ is the fluid velocity with respect to the undisturbed air frame of reference on the LV wall surface which is the sum of $\mathbf{v}^{\text{gust}}$

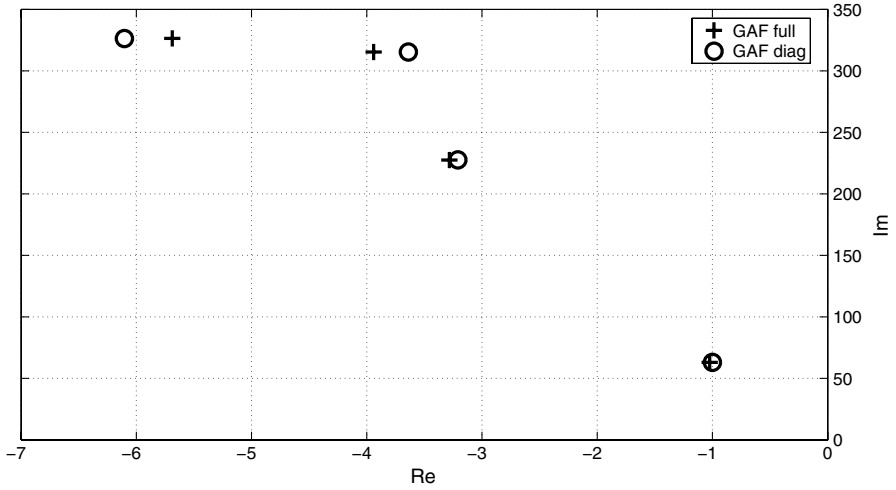

a) Aeroelastic poles of LYRA LV for complete GAF matrix and for diagonalized GAF matrix

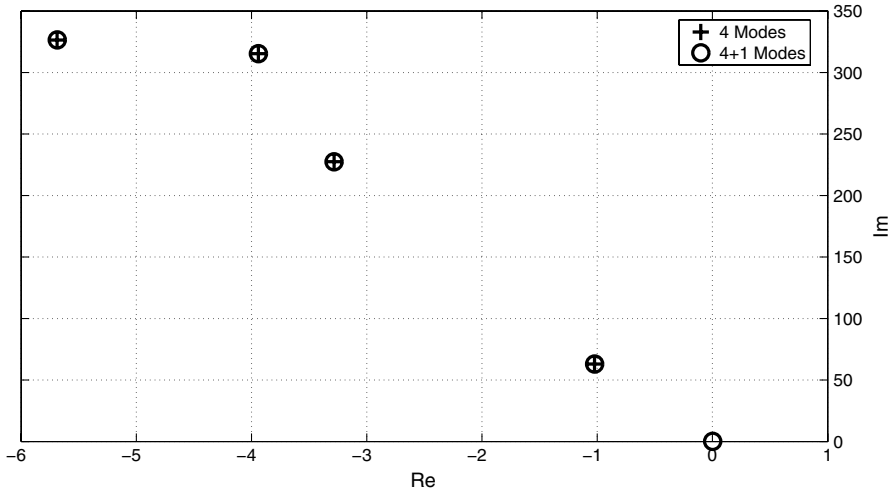

b) Aeroelastic poles of LYRA LV using the first 4 elastic modes and the first 4 elastic modes plus the transverse rigid mode at the given flight conditions.

Fig. 8 Aeroelastic poles of LYRA LV.

and $\mathbf{v}^{\text{mot}}$. The latter represents the fluid velocity induced by the LV motion, which contribution is responsible for the aeroelastic feedback. Accordingly, the normal component on LV surface of $\mathbf{v}^{\text{mot}}$ is given by

$$\mathbf{v}^{\text{mot}} \cdot \mathbf{n} = \mathbf{v}_B \cdot \mathbf{n} - \mathbf{v}^{\text{gust}} \cdot \mathbf{n} = \mathbf{v}_B \cdot \mathbf{n} - \mathbf{k} \cdot \mathbf{n} w \tag{14}$$

which represents the unsteady normal wash. It is seen that the first contribution ($\mathbf{v}_B \cdot \mathbf{n}$) on the right hand side of Eq. (14) of such an aerodynamic input is related to the elastic motion of the LV and is transformed into an aerodynamic force by the GAF matrix term in Eq. (1). The second contribution ($-\mathbf{k} \cdot \mathbf{n} w$) to the aerodynamic input is related to the gust. Indeed, the transverse gust contribution to the boundary conditions is equivalent to that of a rigid mode with a speed $w(t)$ in the opposite direction for the gust. Therefore, the identification of the gust vector f^{gust} in Eq. (1) as a function of the gust profile $w(t)$ may be obtained in the same way as that for the GAF matrix operator. Thus, the main difference between the previous identification procedure for the GAF operator [17] is the addition of the new gust operator, $-\mathbf{k} \cdot \mathbf{n} w(t)$, for the forces acting on the LV, thereby allowing for transverse motion of the LV. Specifically, the input trial function $\tilde{q}_m^t(t)$ is associated with the displacement of the m-th mode in the GAF identification procedure, whereas the input trial function $\tilde{w}^t(t)$ of the gust operator identification is associated to the speed of the rigid transverse motion of the LV. The linearized unsteady gust operator in the Laplace domain transforms the prescribed lateral gust profile $\tilde{w}$ into the generalized gust force vector $\tilde{\mathsf{f}}^{\text{gust}}$ described by:

$$\tilde{\mathsf{f}}^{\text{gust}}(s) = q_D \mathsf{e}^{\text{gust}} \tilde{w} \tag{15}$$

in which $\mathsf{e}^{\text{gust}}(s)$ is the aerodynamic unit gust vector yet to be identified. Thus, assuming a transverse trial component $\tilde{w}^t$ of the gust velocity profile and a rigid motion of the aerodynamic mesh, the corresponding pressure coefficient field $C_p^{\text{gust}}(\xi^\alpha, t)$ can be evaluated by employing a CFD code when the steady pressure field contribution is filtered out. Consequently, the n-th component $f_n^{\text{gust}}(t)$ of the gust vector $\mathsf{f}^{\text{gust}}(t)$ can be evaluated by the same procedure as Eq. (5) was obtained, namely

$$f_n^{\text{gust}}(t) = -q_D \oiint_S C_p^{\text{gust}}(\xi^\alpha, t) \mathbf{n} \cdot \mathbf{\Psi}^{(n)}(\xi^\alpha) \, \mathrm{d}S \tag{16}$$

After transforming this force into the Laplace domain, the gust vector can be identified by the output/input ratio in the Laplace domain, as

$$e_n^{\text{gust}}(s) = \frac{\tilde{f}_n^{\text{gust}}}{\tilde{w}^t q_D} \tag{17}$$

The trial input function $\tilde{w}^t$ has to satisfy the same characteristics as the trial input function $\tilde{q}_n^t$ above. To this end, the same function is used for $w^t(t)$ as it has been used for $q_n^t(t)$, by writing Eq. (7) as

$$w^t(t) = B e^{-[(t-\frac{T}{2})/\kappa T]^2} \tag{18}$$

The amplitude parameter B has been chosen so as to restrain the local angle of attack to a maximum of 1°. The unit gust vector e^{gust} can now be determined and, consequently, a linearized frequency response matrix of the aeroelastic system to a gust is given by rearranging Eq. (1) as

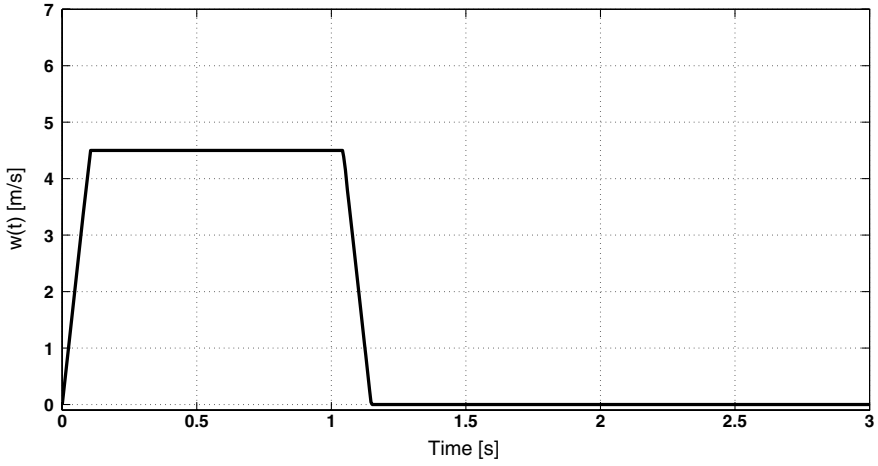

a) First gust profile

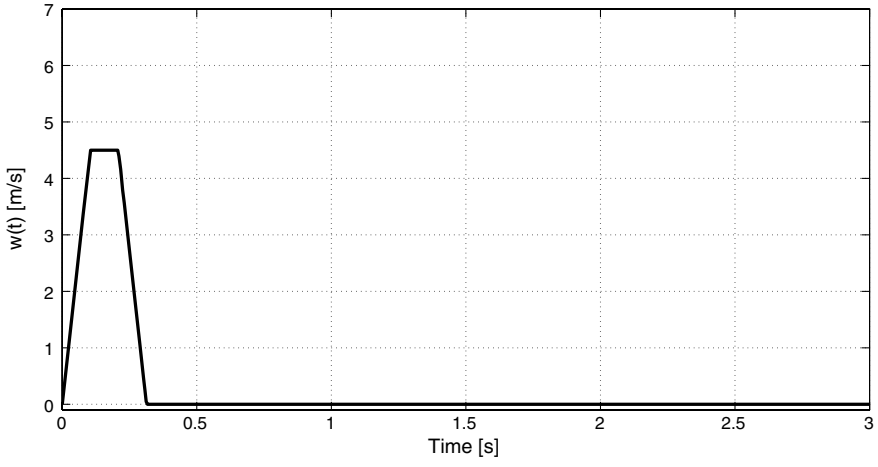

b) Second (more impulsive) gust profile

Fig. 9 Prescribed frozen gust profile as function of time.

$$\mathsf{h}(\omega) = q_D[-\omega^2\mathsf{M} + j\omega\mathsf{D} + \mathsf{K} - q_D\mathsf{E}(\omega; M_\infty, U_\infty)]^{-1}\mathsf{e}^{\text{gust}}(\omega; M_\infty, U_\infty) \tag{19}$$

in which the parametric dependence of the aerodynamic operators to the flight conditions are clearly seen in the aerodynamic terms. Therefore

$$\tilde{\mathsf{q}}(\omega) = \mathsf{h}(\omega)\tilde{w}(\omega) \tag{20}$$

so that the linearized dynamic aeroelastic gust response in terms of $\tilde{\mathsf{q}}(\omega)$ can be obtained by multiplying the transfer function matrix $\mathsf{h}(\omega)$ by the gust input $\tilde{w}$. Note also that once $\mathsf{h}(\omega)$ is known, the other quantities such as, for example, the displacements, can be easily evaluated from Eq. (2).

IV. Matched-Filter Theory

Papoulis [20] originally developed the MFT to obtain the maximum output response for an input $x^{(M)}(t)$ with a prescribed energy level acting on a system with an impulsive response $h(t)$. This theory was applied to a continuous gust analysis of aircraft [21] and for aeroelastic sensitivity analyses [22]. The main advantage of MFT in engineering applications is guaranteed to identify the worse-case response for a given energy level of an input signal.

More specifically, in the present case the MTF can be applied in the design phase of a LV to evaluate the worst-case response of the linearized gust response model. Indeed, the worst possible response is usually of interest so that an appropriate control strategy can be developed. The essential elements of the theory are outlined to aid in the understanding of the outcome. Consider an aeroelastic system with a single input and multiple outputs, for example, a LV passing through a gust input. Let $x(t)$ be the input, $y(t)$ a selected component of the output, and $h(t)$ the impulsive pulse response associated with the selected input/output channel. The MFT yields that the input $x^{(M)}(t)$ matched to the selected output is

$$x^{(M)}(t) = h(t_0 - t)/k \quad \text{or in frequency domain } \tilde{x}^{(M)} = H^* e^{-j\omega t_0}/k \tag{21}$$

in which t_0 is the final instant of time of input application, $*$ indicates complex conjugate, k is a scale factor given by

$$k = \sqrt{\varepsilon_h/\varepsilon_x^{(M)}} \tag{22}$$

with the time signal energy $\varepsilon_x^{(M)}$ given by

$$\varepsilon_x^{(M)} := \int_{-\infty}^{+\infty} x^{(M)^2}(t)\,\mathrm{d}t \equiv \int_{-\infty}^{+\infty} \tilde{x}^{(M)}\tilde{x}^{(M)^*}\frac{\mathrm{d}\omega}{2\pi} \tag{23}$$

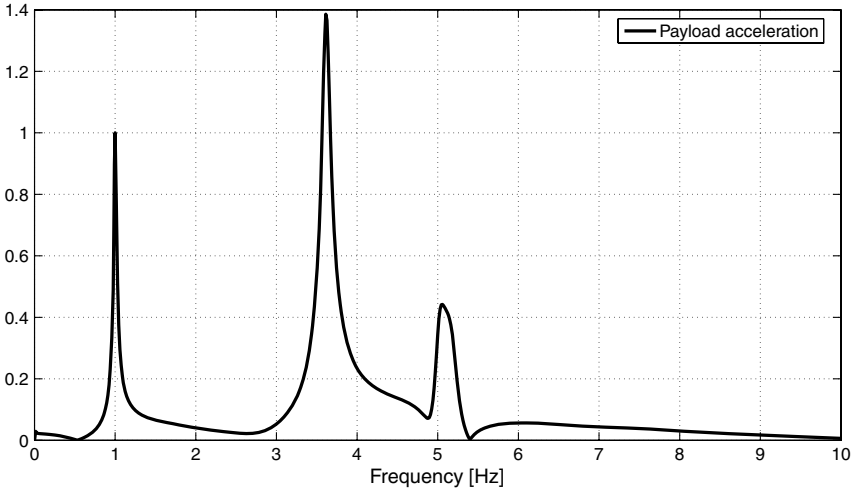

a) Magnitude of the frequency response of the transverse acceleration of the PL grid point

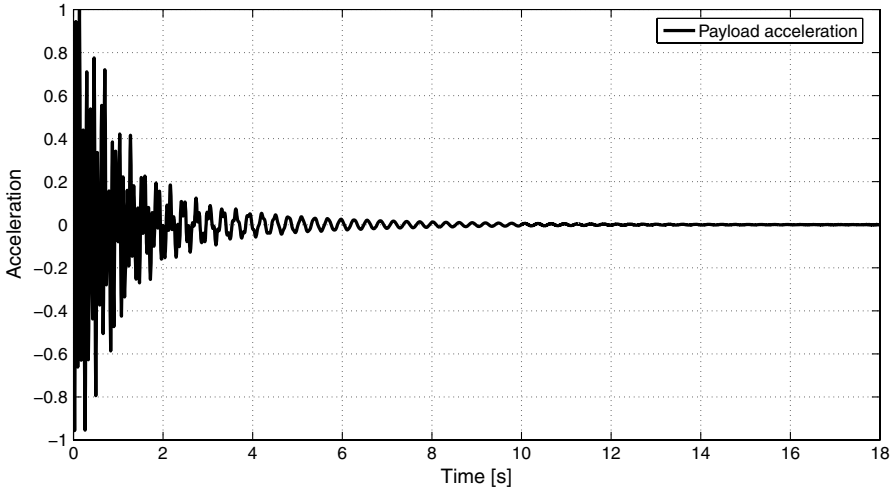

b) Time domain response for the transverse acceleration of the PL grid point

Fig. 10 Response for the normalized transverse acceleration of the PL grid point due to first gust profile.

and the energy associated to the impulse response $h(t)$, ε_h, given by

$$\varepsilon_h := \int_{-\infty}^{+\infty} h^2(t)\,\mathrm{d}t \equiv \int_{-\infty}^{+\infty} H(\omega)H^*(\omega)\frac{\mathrm{d}\omega}{2\pi} \tag{24}$$

Let us consider the corresponding output $y^{(M)}(t)$. The word "matched" has to be understood in the sense that for each input $x^{(M)}(t)$ there is a value for the output at time t_0 that is the maximum in two point of view. First, the maximum value of the time output function $y^{(M)}(t_0)$, and, secondly, it is the maximum with respect to all of the outputs corresponding to the input with the same signal energy $\varepsilon_x^{(M)}$. This maximum value can be analytically shown to be [22]

$$y^{(M)}(t_0) = \sqrt{\frac{\varepsilon_x^{(M)}}{2\pi}\int_{-\infty}^{+\infty} H(\omega)H^*(\omega)\,\mathrm{d}\omega} \tag{25}$$

The expression in Eq. (25) is used to estimate the worse-case scenario of the response (in the meaning specified earlier) on the basis of the knowledge of the input signal energy, that is, $\varepsilon_x^{(M)}$, and of the characteristics of the systems, that is, the gust transfer function matrix component $h_n(\omega)$ [Eq. (19)], in the case considered in the present paper.

The problem has now been fully specified so that a numerical solution of aeroelastic stability of an elastic LV in supersonic flight in presence of gust may be performed to.

V. Numerical Results

The presented approach has been applied to study the linearized stability and gust response analyses of the LYRA LV in a supersonic flight. All the preliminary analyses required for the aeroelastic study follow (Sec. V.A). In particular, the definition of the reference modal basis, the mesh sensitivity for the aerodynamic analysis, the definition of steady-state aerodynamic field are discussed. In Secs. V.B and V.C the aeroelastic stability and response analyses, respectively, are presented.

A. Modal Basis, Steady Aerodynamic Results, and Mesh Sensitivity

The mode selection has been conducted on the assumption that the modes that have the highest percentage of elastic energy associated with the elements of the LV in contact with the external aerodynamic flow are of greatest interest. Further, a frequency band cutoff has been adopted, limiting the analysis to a frequency band width equal to 8 times the first bending natural frequency of the LV. As shown in Table 1, four bending modes satisfy this criterion. Note that due to the axial symmetry of the LV, two identical and geometrically orthogonal bending modes are associated with each natural eigenfrequency. Therefore, in the following, the analysis is conducted by using four pairs of bending modes. The corresponding mode shapes are presented in Fig. 1 where they are represented using a sticklike model. Indeed, the LV structural FE model has been condensed onto the axis of the LV from the detailed FE model, with the use of the

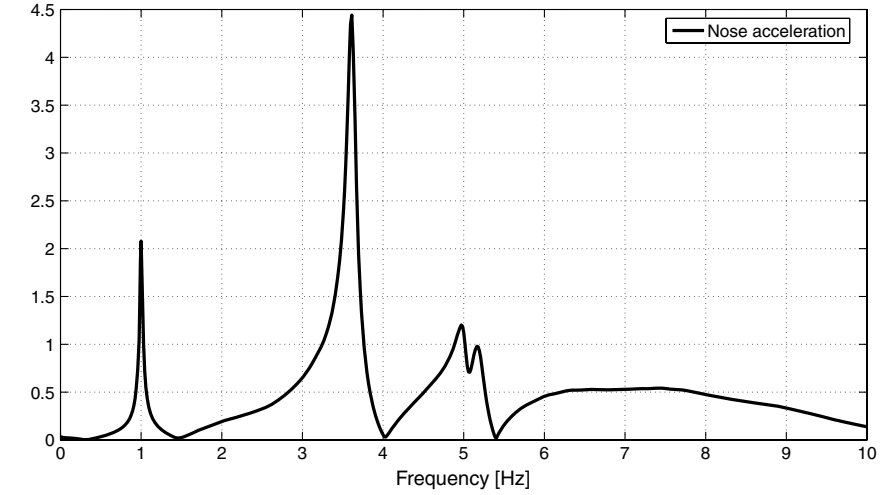

a) Magnitude of the frequency response of the transverse acceleration of the nose grid point

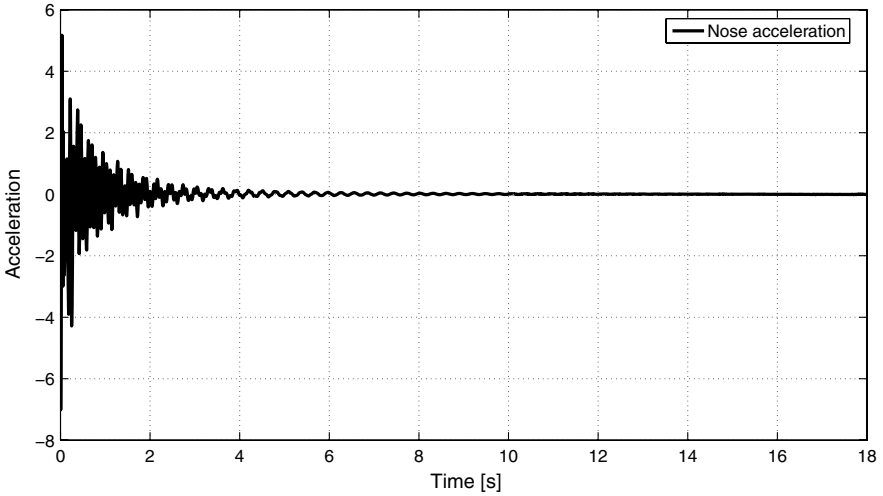

b) Time domain response for the transverse acceleration of the nose grid point

Fig. 11 Response for the normalized transverse acceleration of the nose grid point due to first gust profile: normalization factor is based on maximum PL acceleration (see Fig. 10).

standard superelement technique. Once the displacement given by the mode shape has been obtained for each of the sticklike modal representations, it is projected on the LV surface, thereby changing its surface geometry. An example of surface deformation caused by the first mode on the mesh of the LYRA LV is depicted in Fig. 2. The projection of the modal displacement field from the sticklike model is performed on the centers of the aerodynamic surface elements for aerodynamic force projections as well as on the nodes of the same aerodynamic surface panel for imposing the unsteady boundary conditions.

As a second preliminary activity, a mesh-sensitivity study was performed on both the steady and unsteady problems. Indeed, the need for also conducting a mesh-sensitivity analysis for the unsteady problem is due to the great importance played by the unsteady issues of the problem in the aeroelastic analysis. A detailed study on the computational domain shape and size were conducted in [18] and it is not repeated here for the sake of conciseness.

The reference flow conditions under consideration are: Mach number $M_\infty = 2.15$, $U_\infty = 628.62$ m/s, and $\rho_\infty = 0.284$ kg/m^3. The angle of attack has been fixed at $\alpha = 1^\circ$ and it is defined as the angle between the LV axis in the undeformed configuration and the direction line of the undisturbed flow. The steady static pressure field evaluated is reported in Fig. 3, in which the mesh sensitivity analysis is also presented. The aerodynamic field is evaluated using the inviscid implicit steady solver in the code Fluent [23]. The mesh-sensitivity analysis of the unsteady problem has been conducted in the following way: first, the steady component has been filtered out from the unsteady solution, then the resulting pressure disturbances have been projected on every assumed modal shape so as to obtain the generalized aerodynamic forces $e_n^{(m)}(t)$. The generalized Lagrangian forces thereby obtained in the time domain have been calculated for all the assumed modes [see Eq. (5)], including the rigid one associated to the gust analysis [see Eq. (16)]. However, assuming LV axis to be the x-axis, the effects of motion associated with any given mode in the y-direction corresponding to a mode along the z-direction (and vice versa) proved to be quite small. Thus, only four elastic modes, instead of eight, all in the same direction, have been considered in the present analysis. The first part of the unsteady aerodynamic modeling consists of a number of unsteady aerodynamic time marching simulations, equal to the number of the assumed modes. The unsteady pressure coefficient $C_{p_n}^{\text{mot}}(\xi^\alpha, t)$ are calculated from the solution of the Euler equations with boundary conditions obtained from the mode shapes. Similarly, the $C_p^{\text{gust}}(\xi^\alpha, t)$ field is generated from the boundary conditions obtained from the rigid transverse mode. Then, the corresponding generalized forces $e_n^{(m)}(t)$ and $f_n^{\text{gust}}(t)$ are calculated from Eqs. (5) and (16).

The effect of using three different mesh sizes on the generalized forces $e_n^{(m)}(t)$ is shown in Fig. 3 for the steady case and in Figs. 4 and 5 for the unsteady case. The same kind of mesh sensitivity result, but this time only for E_{11}, the first component of GAF matrix representing the unsteady aerodynamic coefficient, is shown in

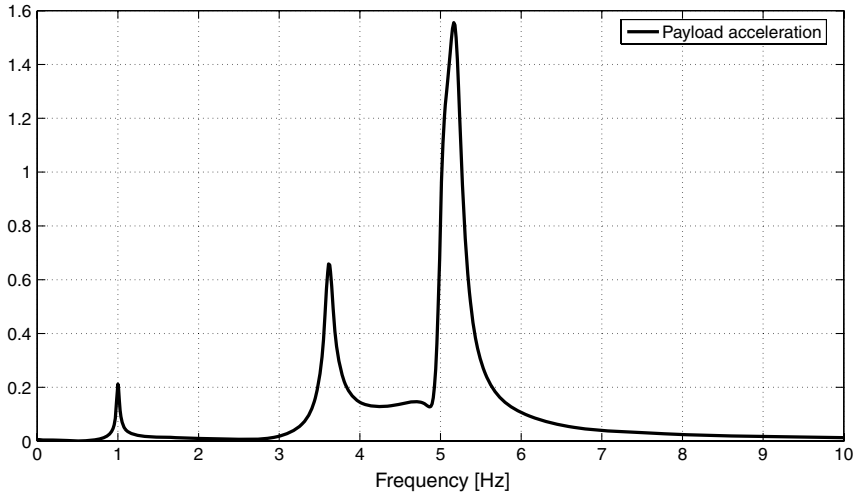

a) Magnitude of the frequency response of the transverse acceleration of the PL grid point

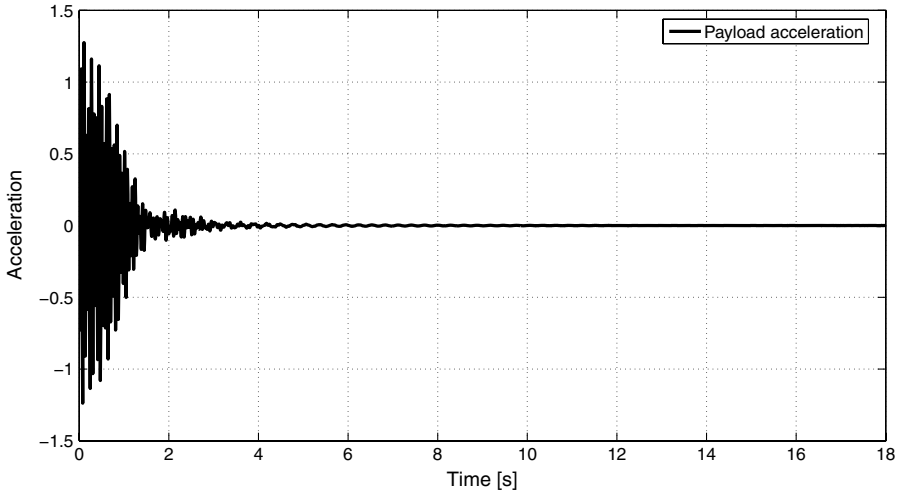

b) Time domain response for the transverse acceleration of the PL grid point

Fig. 12 Response for the transverse acceleration of the PL grid point due to second gust profile: normalization factor is based on maximum PL acceleration (see Fig. 10).

Fig. 6. The quantities in Fig. 6 are functions of the reduced frequency k, defined as $k := \omega D/U_\infty$, in which D is the reference length for the LV section, namely the diameter. It is clear from these figures that meshes B and C are equally suitable for the numerical simulations. On the other hand, when the steady-state reference pressure distribution shown in Fig. 3 is also considered, the mesh size when mesh C is employed leads to the more converged solution in regions of large gradient in the diameter of LV. For this reason, mesh C should be selected for both the steady and unsteady simulations.

As final comment, some considerations on computational costs need to be pointed out. The three meshes mentioned above have 3×10^5, 6×10^5, and 12×10^5 fluid cells, respectively. The computational hardware consisted of five dual-core processors each with 3 Gb of RAM. With this configuration, mesh C required approximately 24 hours of CPU time for each mode simulation. Since this computational effort is acceptable, mesh C was adopted for all the simulations.

B. Stability Analysis

The flight condition considered in the present analysis is a supersonic flow ($M_\infty = 2.15$), whereas in [17,18]a transonic flight was analyzed. An iterative procedure [5,7] has been employed to obtain the aeroelastic poles s_n using Eq. (8) at the prescribed flight conditions of LYRA LV. The aeroelastic poles obtained when only the first four modes of Table 1 are included in the presence of a structural damping ratio $\zeta = 0.01$ for all the four modes used in the analysis is presented in Table 2. In Fig. 7 the evaluated poles are compared with those obtained considering only one ($N = 1$), two ($N = 2$), three modes ($N = 3$) and all four Lagrangian coordinates in the aeroelastic stability analysis [Eq. (1)]. The figure shows that in this case the analysis with a low number of modes is shown to be conservative in terms of the stability analysis.

Moreover, Fig. 8a shows the same stability analysis compared with that carried out considering only the diagonal term of the GAF matrix, namely, neglecting the unsteady aerodynamic coupling in the linearized operator. The figure shows that this simplification may be conservative for some poles but not-conservative for others and, therefore, it is here recommended not to be adopted in the stability analysis of a LV. The inclusion of the transverse plunge rigid mode in the aeroelastic analysis does not affect the stability scenario: indeed, in Fig. 8b the previous results are compared with those obtained including the transverse rigid mode in the stability analysis, namely including the proper row and column in the GAF matrix and no differences are observed.

C. Gust Response Analysis

The gust response analysis is the novel modeling and results contribution of the present work with respect to [17,18]. A transverse gust response analysis has been carried out considering a possible gust input shown in Fig. 9a which was proposed by the AVIO company, the VEGA LV manufacturer, as typical for LVs. Specifically, for the function $w(t)$ a trapezoidal profile with a

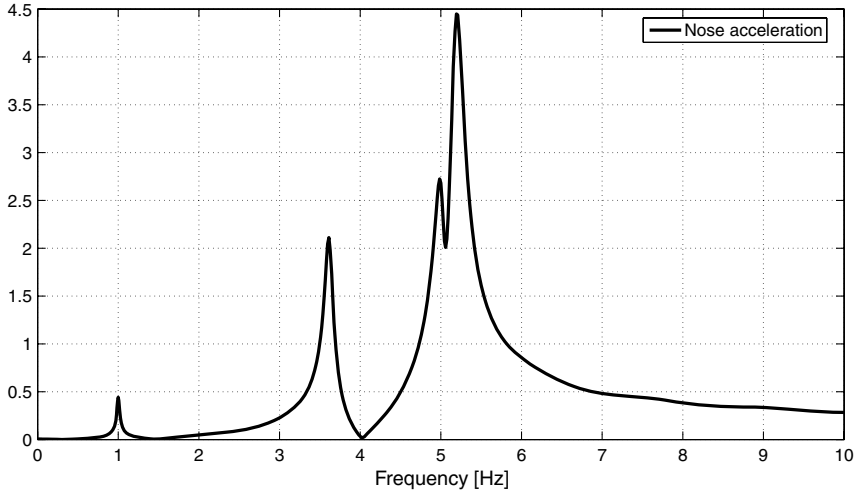

a) Magnitude of the frequency response of the transverse acceleration of the PL grid point

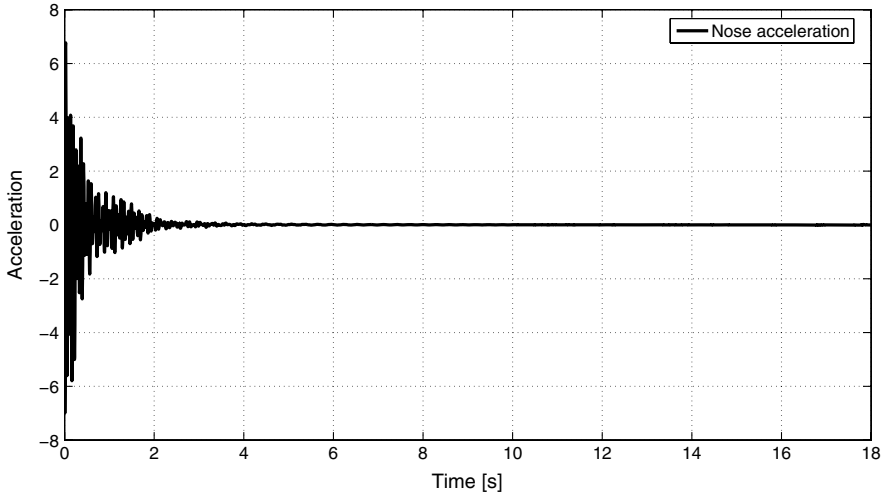

b) Imaginary part of the first column entries of the GAF matrix in frequency domain

Fig. 13 Response for the transverse acceleration of the nose grid point to second gust profile: normalization factor is based on maximum PL acceleration (see Fig. 10).

maximum value of 4.5 ms^{-1} has been assumed but, for the second profile, Fig. 9b, a more impulsive input having a smaller time window has been also used (Fig. 9b). The time inputs have been transformed from the time domain to the frequency domain by using fast Fourier transform. Then, Eq. (20) is used to obtain the output vector in the frequency domain. The discrete Fourier transform strategy consisted of the use of a number of time samples equal to 4096 and a time sampling rate of $\Delta t = 0.0048$ s, which yields a frequency resolution of $\Delta f = 0.050$ Hz $= 1/(\Delta t 4096)$ Hz. The components of the frequency spectrum have sufficient energy to excite the frequency band including the modes considered in the present analysis.

The results for the first input gust are shown in Figs. 10 and 11 in terms of transverse vibration of the payload (PL) FE node and LV-nose FE node. The results have been scaled to have a maximum peak value equal to 1 both in frequency and time domain for the PL case shown in Fig. 10. It should be noted that there are resonant responses for all the modes included in the calculation. The largest response occurs at the second mode. It can be seen by comparing Fig. 10 with Fig. 11 that the vibration levels resulting from the aeroelastic LV interaction with the gust are significantly larger for the nose cone than for the payload. However, the aeroelastic damping during the given flight conditions practically cancels the effects of the gust perturbation after approximately ten seconds. Indeed, note that we should have used a larger structural damping coefficient in view of the considerable presence of the grain materials inside the solid rocket motors. This modeling aspect has not been considered in the present analysis for conservative reasons but, if it were included, then probably, the oscillation time of 10 s would be further reduced.

Figures 12 and 13 show the results for the second input gust in term of vibration of the PL FE node and LV-nose FE node. It should be again noted that there are resonant response for all the modes included in the calculation. However, the largest response occurs for the last two modes included in the analysis. This may be seen by comparing Fig. 13 with Fig. 12: the vibration levels resulting from the aeroelastic LV interaction with the gust are significantly larger for the nose cone than for the payload. However, in this case the aeroelastic damping virtually cancels the effects of the gust perturbation after approximately four seconds. The previous comment on the possible damping influence of the grain in the response may be again addressed also in the present case. It is worth pointing out that, during the vibration qualification tests for launch, it is typically verified that PLs have resonance peaks beyond a given frequency (approximately 50 Hz for a typical LV). Also, they should have maximum acceleration peaks below approximately 10 g. The gust response vibratory levels obtained have a frequency content below before the mentioned frequency band limit. Moreover, the maximum peaks reached are lower than those of the qualification tests, thereby showing that the gust environment studied induces a mechanical burden on the PL which is lower than that expected in the qualification test (as this typically due to the propulsion system during the firing phase). Note also that applying in an inverse way the proposed methodology, a gust input producing a vibration level equal

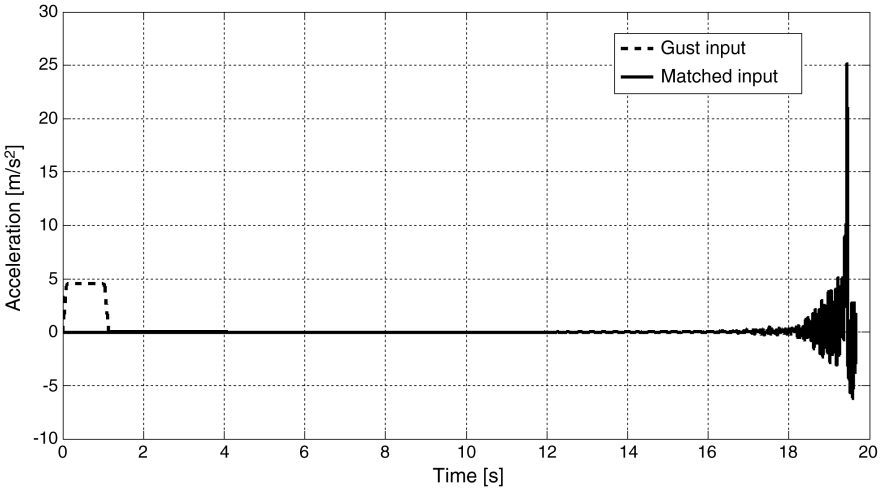

a) Energy-equivalent worst-matched input for the gust response problem

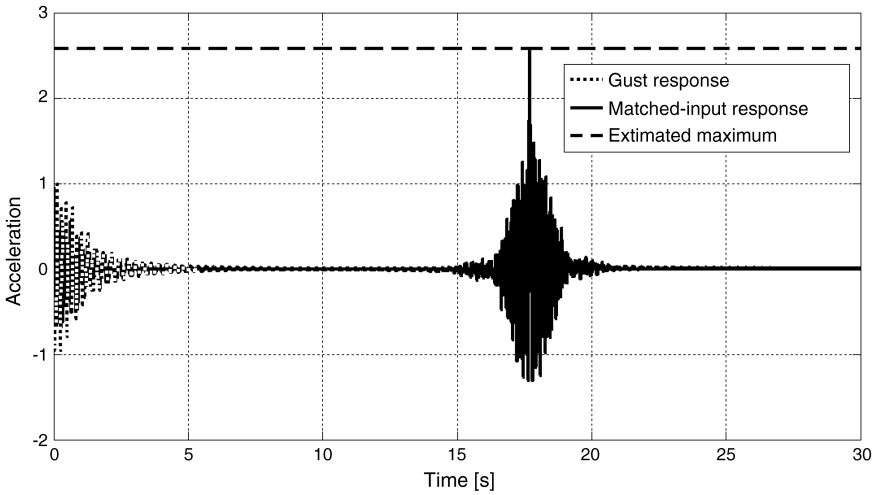

b) Gust responses acceleration to the prescribed gust input, to the energy-equivalent worst-matched input and the estimated peak level

Fig. 14 MFT theory application.

to that of the qualification test level could be identified, so as to verify the comparability with feasible turbulence conditions.

Finally, Fig. 14 shows the MFT application on the aeroelastic gust response of the PL to the worst-case scenario. Specifically, Fig. 14a presents the first gust input considered (Fig. 9a) along with the *matched input*, (that is, the gust input having the same rms as the given input signal, but giving the highest peak in the time response among all the response due to input with the same energy content). Next, in Fig. 14b the ensuing time PL response to the given input is compared with that induced by the worst matched input [Eq. (21)] and also with the response maximum threshold which has been estimated from Eq. (25). Note that this theory is really an effective tool in the design process to estimate the worst-case response scenario for a prescribed energy of the signal input.

VI. Conclusions

The theory previously developed for the prediction of vibrations and stability of an LV moving at a transonic speed has been extended to supersonic flights that are subject to transverse gusts.

The procedure has been successfully applied to the flight of LYRA LV at a Mach number $M_\infty = 2.15$ in two different gust scenarios. It is shown that the aeroelastic response of the vehicle is different at supersonic speed from that at transonic speed. Further, different gust types, characterized by the narrowness of the signal input shape, induce quite different frequency responses of the vehicle. The method has been further extended to include the analysis of worst-case scenario responses. The predictions are conservative in the sense that the damping factor used in the calculation consists solely of structural damping without consideration of the effects of other components of the LV (e.g., grain materials).

The proposed methodology is considered to be a valuable tool for the aeroelastic analysis of a launch vehicle subjected to a transverse gust and, therefore, for LV design.

Acknowledgments

This paper has been supported by an Avio S.p.A grant entitled Modeling and Analysis of Stability and Gust Response Linearized Around an Atmospheric Flight Condition: Application on LYRA LV. The authors thank John A. Reizes for his helpful suggestions in the progress of the present work.

References

[1] Bisplinghoff, R. L., Ashley, H., and Halfman, R. L., *Aeroelasticity*, Addison–Wesley, Cambridge, MA, 1955, pp. 1–14, 527–626.

[2] Morino, L., "A General Theory of Unsteady Compressible Potential Aerodynamics," NASA CR-2464, 1974.

[3] Dowell, E. H., *A Modern Course in Aeroelasticity*, Kluwer Academic, Norwell, MA, 1995.

[4] Silva, W. A., Hong, M. S., Bartel, L. E., Piatak, D. J., and Scott, R. C., "Identification of Computational and Experimental Reduced-Order Models," *Proceedings of International Forum on Aeroelasticity and Structural Dynamics*, Netherlands Ass. of Aeronautical Engineers Paper No. 2003-US-39, June 2003.

[5] Hassig, H. J., "An Approximate True Damping Solution of the Flutter Equation by Determinant Iteration," *Journal of Aircraft*, Vol. 8, No. 11, 1971, pp. 885–889. doi:10.2514/3.44311

[6] Morino, L., Mastroddi, F., De Troia, R., Ghiringhelli, G. L., and Mantegazza, P., "Matrix Fraction Approach for Finite-State Aerodynamic Modeling," *AIAA Journal*, Vol. 33, No. 4, 1995, pp. 703–711. doi:10.2514/3.12381

[7] Gennaretti, M., and Mastroddi, F., "A Study of Reduced-Order Models for Gust-Response Analysis of Flexible Fixed Wing," *Journal of Aircraft*, Vol. 41, No. 2, March–April 2004, pp. 304–313. doi:10.2514/1.9325

[8] Rodden, W. P., and Johnson, E. H., MSC/NASTRAN Aeroelastic Analysis, Users' Guide V68, The MacNeal–Schwendler Corporation, 1994.

[9] Ragab, M. M., "Buffet Loads Prediction for a Launch Vehicle and Comparison to Flight Data," *Journal of Spacecraft and Rockets*, Vol. 29, No. 6, 1992, pp. 849–855. doi:10.2514/3.25541

[10] Reding, P. J., and Ericsson, L. E., "Hammerhead and nose-cylinder-flare Aeroelastic Stability Revisited," *Journal of Spacecraft and Rockets*, Vol. 32, No. 1, 1995, pp. 55–59. doi:10.2514/3.26574

[11] Dotson, K. W., Baker, R. L., and Sako, B. H., "Launch Vehicle Self-Sustained Oscillation from Aeroelastic Coupling Part 1: Theory," *Journal of Spacecraft and Rockets*, Vol. 35, No. 3, 1998, pp. 365–373. doi:10.2514/2.3336

[12] Dotson, K. W., Baker, R. L., and Bywater, R. J., "Launch Vehicle Self-Sustained Oscillation from Aeroelastic Coupling Part 2: Analysis," *Journal of Spacecraft and Rockets*, Vol. 35, No. 3, 1998, pp. 374–379. doi:10.2514/2.3337

[13] Karpel, M., Yaniv, S., and Livshits, D. S., "Integrated Solution for Computational Static Aeroelasticity of Rockets," *Journal of Spacecraft and Rockets*, Vol. 35, No. 5, 1998, pp. 612–618. doi:10.2514/2.3393

[14] Ericsson, L. E., "Hammerhead Wake Effects on Elastic Vehicle Dynamics," *Journal of Spacecraft and Rockets*, Vol. 34, No. 2, 1997, pp. 145–151. doi:10.2514/2.3193

[15] Ericsson, L. E., and Pavish, D., "Aeroelastic Vehicle Dynamics of a Proposed Delta II 7920-10L Launch Vehicle," *Journal of Spacecraft and Rockets*, Vol. 37, No. 1, 2000, pp. 28–38. doi:10.2514/2.3546

[16] Ericsson, L. E., "Unsteady Flow Separation can Endanger the Structural Integrity of Aerospace Launch Vehicle," *Journal of Spacecraft and Rockets*, Vol. 38, No. 2, 2001, pp. 168–179. doi:10.2514/2.3690

[17] Capri, F., Mastroddi, F., and Pizzicaroli, A., "A Linearized Aeroelastic Analysis for a Launch Vehicle in Transonic Flow," *Journal of Spacecraft and Rockets*, Vol. 43, No. 1, Jan–Feb 2006, pp. 92–104. doi:10.2514/1.13867

[18] Mastroddi, F., Stella, F., Polli, G. M., and Giangi, M., "Sensitivity Analysis for the Dynamic Aeroelasticity of a Launch Vehicle," *Journal of Spacecraft and Rockets*, Vol. 45, No. 5, Sept.–Oct. 2008, pp. 999–1009. doi:10.2514/1.30725

[19] Mastroddi, F., Polli, G. M., and Rinaldi, S., "A Reduced-Order Modeling for the Aeroelastic Analysis of a Launch Vehicle," *Proceedings of International Forum on Aeroelasticity and Structural Dynamics, IFASD 2007*, Swedish Ass. of Aeronautical Engineers Paper No. 2007-IF-101, June 2007.

[20] Papoulis, A., "Maximum Response with Input Energy Constraints and the Matched Filter Principle," *IEEE Transactions on Circuit Theory*, Vol. 17, No. 2, 1970, pp. 175–182. doi:10.1109/TCT.1970.1083078

[21] Pototzky, A. S., Zeiler, T. A., and Perry, B. III, "Calculating Time-Correlated Gust Loads Using Matched Filter and Random Process Theory," *Journal of Aircraft*, Vol. 28, No. 5, 1991, pp. 346–352. doi:10.2514/3.46033

[22] Balis Crema, L., Mastroddi, F., and Coppotelli, G., "Aeroelastic Sensitivity Analyses for Flutter Speed and Gust Response," *Journal of Aircraft*, Vol. 37, No. 1, 2000, pp. 172–180. doi:10.2514/2.2577

[23] Fluent 6.2, User's Guide, Fluent.Inc, Jan. 2005.

M. Costello
Associate Editor